Lasers in Medical Science (2019) 34:615–628
https://doi.org/10.1007/s10103-018-2639-x

ORIGINAL ARTICLE

Potentials and pitfalls of gold-silica nanoshell as the exogenous contrast agent for optical diagnosis of cancers: a numerical parametric study

Xiao Xu[1]

Received: 22 May 2018 / Accepted: 11 September 2018 / Published online: 22 October 2018

Abstract

For nanoshell-assisted optical detection of cancers, gold shell, silica core (gold-silica) nanoshells are engineered to be the exogenous contrast agent. This work has performed systematic numerical parametric study to investigate the nonlinear dependences of the hemisphere diffuse reflectance on gold-silica nanoshells, laser irradiance, and hosting biology tissue. Planar phantom based tissue models have been constructed as platforms for study. The radiant transport equation (RTE) has been applied to mathematically describe the interactions among laser lights, hosting tissues, and hosted nanoshells. The diffuse reflectance signal under various combinations of parametric conditions has been computed and analyzed. Parametric parameters whose effects on the diffuse reflectance signal have been investigated are: (1) optical properties of a nanoshell generic, (2) nanoshell volume fraction, which is an indicator of nanoshell accumulation in the target tissue site, (3) the width of irradiating laser beam, and (4) thickness of the tissue slab. Seven nanoshell generics have been tested as the exogenous contrast agent including the $R[50, 10]$ (radius of silica core is 50 nm and thickness of gold shell is 10 nm), $R[55, 25]$, $R[40, 15]$, $R[40, 40]$, $R[104, 23]$, $R[75, 40]$ and $R[154, 24]$ nanoshells. It has been found the $R[55, 25]$ nanoshell works best as the exogenous contrast agent, the $R[75, 40]$ and $R[104, 23]$ nanoshells show good potentials as well while the $R[50, 10]$ and $R[40, 15]$ nanoshells should be avoided for diagnostic usage. The practice of neglecting the absorption characteristic of the exogenous contrast agent, which is quite common among the bio-nano community, has been proven to end up with an over-prediction of the effectiveness of the exogenous contrast agent. Such practice therefore is not well justified and should be avoided in future research. Interactions among laser lights, the tissue and nanoshells are highly nonlinear, demonstrated by that nanoshell generics with totally different optical properties might have similar effects on the diffuse reflectance signal and vice versa. Prior to any bench experiment, preliminary numerical investigation as this work has showcased is highly recommended.

Keywords Optical imaging · Cancer detection · Gold-silica nanoshell · Lasers

Introduction

Optical imaging is a broad category. Optical confocal microscopy (OCM) [1, 2], optical coherence tomography (OCT) [3–7, 18], diffuse reflectance spectroscopy [8, 9, 19], and diffuse optical tomography (DOT) are all branches of it. Compared to conventional imaging modalities such as magnetic resonance imaging (MRI) and positron emission tomography (PET), optical imaging modalities enable detective laser lights to penetrate into the target object as deep as several hundred micro-meters (μm) and non-invasively capture images with a resolution of μm. Such resolution is 1 to 2 orders finer than what MRI is able to achieve [10, 19]. The rapid development of optical modalities during the past decades has injected new hopes to big advancements in the cancer detection technique, particularly the early-staged cancer detection, which is notoriously challenging mainly because disease signatures are typically very subtle.

For optical imaging modalities, it is a common practice to use exogenous contrast agents to enhance the contrast between healthy and cancerous tissues. The diffuse

✉ Xiao Xu
xiao717@gmail.com

[1] Present address: School of Mechanical and Electrical Engineering, Guilin University of Electronic Technology, Guilin, People's Republic of China

reflectance signal, which is of essential importance for detective imaging, is recognized as the macroscopic display of interactions among detective laser lights, tissue medium within which the lights propagate and the exogenous contrast agent. By controlling factors such as generics and target-specific accumulation of the exogenous contrast agent, it is expected that the exogenous contrast agent could affect the diffuse reflectance signal in such a way that it is desirable for diagnostic goals.

Organic dyes were the first generation of exogenous contrast agent. The toluidine blue [20], Lugol's iodine [21], and Indocyanine green all have been used for such purpose. With the revolutionary development of nano science and technology, nanoparticles have emerged as new candidates for the exogenous contrast agent [3–18]. Various nanostructures have been tested for such purpose including nanotube, nanoshell, nanorod, nanosphere, and nanocage. Among them, the gold shell, silica-core (gold-silica) nanoshell seems to be particularly promising because of the agile tunability and high efficiency of its optical properties. Compared to organic dyes, plasmonic resonance of the gold-silica nanoshell, which is an important indicator of its optical efficiency, could be tuned to be 4 to 5 orders higher than that of organic dyes [10]. Besides, peak of this particle's plasmonic resonance could easily be tuned to occur in the near-infrared (NIR) spectrum, which is the optical gateway for medicine that allows maximum laser penetration. When used as the exogenous contrast agent, such tunability enables the medical practicer more control over the imaging procedures.

Using gold-silica nanoshell as a reference exogenous contrast agent, and using phantom based tissue models as the study platform, this work has performed systematic parametric study to investigate the nonlinear dependence of the diffuse reflectance on the source laser, the hosting tissue and the exogenous contrast agent. Different nanoshell generics have been tested as the exogenous contrast agent including the *R*[50, 10] (radius of silica core is 50 nm and thickness of gold shell is 10 nm), *R*[55, 25], *R*[40, 15], *R*[40, 40], *R*[104, 23], *R*[75, 40] and *R*[154, 24] nanoshells. As a parametric study, parametric parameters of this work include: (1) optical properties of the nanoshell generic, (2) target-specific nanoshell accumulation, (3) the width of irradiating laser beam, and (4) the thickness of tissue slab. For each parametric parameter, customized study case has been constructed to investigate its effects on the diffuse reflectance signal.

Major objectives of this work are: (1) to shed some lights on how to arrange all controllable factors, including those associated with source laser and those associated with hosting tissue and hosted exogenous contrast agent, to plan an optimized imaging procedure, and (2) to answer the question of what gold-silica nanoshell generic would serve as a good exogenous contrast agent. Within the context of diagnostic imaging, the scattering characteristic of the exogenous contrast agent is the key focus. A common practice among the bio-nano community therefore is simply neglecting the absorption perspective of the exogenous contrast agent and considering its scattering perspective only. There is always a question mark on whether such practice is well justified or not. This work also aims at answering this question.

The rest of this paper is organized in the following order: In "Mathematical modeling," details of mathematical modeling the interactions among laser lights, hosting biology tissue, and hosted gold-silica nanoshells would be presented. In "Results and discussions," details of constructing phantom based tissue models and parametric study cases to investigate effects of various parametric parameters on the diffuse reflectance signal would be investigated. Section "Conclusive remarks" concludes this work, and major findings of this study would be summarized and conclusions would be drawn.

Mathematical modeling

If laser irradiances come from a continuous wave (CW) source, the steady-state, integral-differential radiant transport equation (RTE) [46, 47] could be applied to describe the propagation of laser lights within the turbid tissue medium:

$$\frac{\partial L(\boldsymbol{r},\boldsymbol{s})}{\partial \boldsymbol{s}}+(k_\alpha(\boldsymbol{r})+k_s(\boldsymbol{r}))L(\boldsymbol{r},\boldsymbol{s})=\frac{k_s(\boldsymbol{r})}{4\pi}\int_{4\pi}\Phi(\boldsymbol{s},\boldsymbol{s}')\times L(\boldsymbol{r},\boldsymbol{s}')d\Omega' \quad (1)$$

where $L(\boldsymbol{r},\boldsymbol{s})$ indicates the radiant intensity at position $\boldsymbol{r}$ and in the direction $\boldsymbol{s}$, Ω' indicates the solid angle, kernel function $\Phi(\boldsymbol{s},\boldsymbol{s}')$ indicates the phase function between directions $\boldsymbol{s}$ and $\boldsymbol{s}'$, and $k_\alpha(\boldsymbol{r})$ and $k_s(\boldsymbol{r})$ respectively indicate local absorption and scattering coefficients, which are overall values that take both biology tissue and the exogenous contrast agent into account [22, 23, 25–28]:

$$\begin{aligned} k_\alpha(\boldsymbol{r}) &= k_{\alpha,t}(\boldsymbol{r})+k_{\alpha,exo}(\boldsymbol{r}) \\ k_s(\boldsymbol{r}) &= k_{s,t}(\boldsymbol{r})+k_{s,exo}(\boldsymbol{r}) \end{aligned} \quad (2)$$

where the subscripts "t" and "exo" indicate the biology tissue and the exogenous contrast agent respectively. When gold-silica nanoshell is used as the exogenous contrast agent, $k_{\alpha,exo}(\boldsymbol{r})$ and $k_{s,exo}(\boldsymbol{r})$ could respectively be quantified by nanoshell's absorption and scattering efficiencies Q_α and Q_s:

$$\begin{aligned} k_{\alpha,exo} &= C_\alpha N_T = \pi r_0^2 Q_\alpha N_T \\ k_{s,exo} &= C_s N_T = \pi r_0^2 Q_s N_T \end{aligned} \quad (3)$$

where C_α and C_s respectively indicate the absorption and scattering cross sections, N_T represents the in total number

of nanoshells per unit volume and r_0 represents radius of the silica core. Since nanoshells are spherical, Q_α and Q_s could be approximated by the Mie theory [33].

Since most biological tissues are turbid, the Henyey-Greenstein scattering phase function [32] is a good approximation for $\Phi(\boldsymbol{s}', \boldsymbol{s})$:

$$\Phi(\boldsymbol{s}', \boldsymbol{s}) = \frac{1}{4\pi} \frac{1 - g^2}{[1 + g^2 - 2g\cos(\boldsymbol{s} \cdot \boldsymbol{s}')]^{1.5}} \tag{4}$$

where $g \in [-1, 1]$ is the anisotropy factor. For most biology tissues, g is between 0.7 and 1 [46].

Equation 1 needs to be closed by boundary conditions. For a non-emitting, diffusively reflecting boundary, the corresponding boundary condition is of the following form:

$$L(\boldsymbol{r}, \boldsymbol{s}) = q_0 \delta(\boldsymbol{s} - \boldsymbol{s_c}) + \frac{\rho}{\pi} \int_{\boldsymbol{n} \cdot \boldsymbol{s}' < 0} L(\boldsymbol{r}, \boldsymbol{s}') \left| \boldsymbol{n} \cdot \boldsymbol{s}' \right| d\Omega' \tag{5}$$

where q_0 represents the magnitude of the laser irradiance, $\boldsymbol{s_c}$ represents the direction in which laser light enters the tissue medium, $\boldsymbol{n}$ represents the normal vector of the boundary position $\boldsymbol{r}$, ρ represents the reflectivity of the boundary and δ represents the Dirac-delta function.

Note that $L(\boldsymbol{r}, \boldsymbol{s})$ in Eqs. 1 and 5 is comprised with two parts, namely the remnant of the incoming collimated irradiance, which is identified as $L_c(\boldsymbol{r}, \boldsymbol{s})$ and the induced diffusion radiation, which is identified as $L_d(\boldsymbol{r}, \boldsymbol{s})$:

$$L(\boldsymbol{r}, \boldsymbol{s}) = L_d(\boldsymbol{r}, \boldsymbol{s}) + L_c(\boldsymbol{r}, \boldsymbol{s}) \tag{6}$$

According to the Beer-Lambert law [46], $L_c(\boldsymbol{r}, \boldsymbol{s})$ could be approximated as

$$L_c(\boldsymbol{r}, \boldsymbol{s}) = q_0 \exp(-(k_\alpha + k_s)(\boldsymbol{r} - \boldsymbol{r_b}))\delta(\boldsymbol{s} - \boldsymbol{s_c}) \tag{7}$$

where $\boldsymbol{r} - \boldsymbol{r_b}$ represents the absolute distance the light has traversed after its entrance from the boundary position $\boldsymbol{r_b}$. Substitute Eqs. 6 and 7 to Eq. 1, governing equation for $L_d(\boldsymbol{r}, \boldsymbol{s})$ could be derived as:

$$\begin{aligned} &\frac{\partial L_d(\boldsymbol{r}, \boldsymbol{s})}{\partial \boldsymbol{s}} + (k_\alpha(\boldsymbol{r}) + k_s(\boldsymbol{r})) L_d(\boldsymbol{r}, \boldsymbol{s}) \\ &= \frac{k_s(\boldsymbol{r})}{4\pi} \int_{4\pi} \Phi(\boldsymbol{s}, \boldsymbol{s}') L_d(\boldsymbol{r}, \boldsymbol{s}') d\Omega' + \frac{k_s(\boldsymbol{r})}{4\pi} \Phi(\boldsymbol{s}, \boldsymbol{s_c}) L_c(\boldsymbol{r}, \boldsymbol{s_c}) \end{aligned} \tag{8}$$

The associated boundary condition for $L_d(\boldsymbol{r}, \boldsymbol{s})$ could be derived from Eq. 5:

$$L_d(\boldsymbol{r}, \boldsymbol{s}) = \frac{\rho}{\pi} \int_{\boldsymbol{n} \cdot \boldsymbol{s}' < 0} L_d(\boldsymbol{r}, \boldsymbol{s}') \left| \boldsymbol{n} \cdot \boldsymbol{s}' \right| d\Omega' \tag{9}$$

Equations 8 and 9 require a numerical approximation, for which the finite volume method (FVM) is a well established alternative [22, 23, 29, 30]. An in-house FVM based RTE solver has been developed, which has been verified by legacy reference problems. Details of the verification could be found in [24].

Results and discussions

In this section, various parametric study cases would be constructed and each case is intended to investigate effects of one specific parametric parameter on the diffuse reflectance signal. Two planar, phantom-based tissue models, namely the single-layer tissue model (Fig. 1a) and the dual-layer tissue model (Fig. 1b) would be used as the platform for study. Wavelength of the irradiating laser lights for both tissue models is 830 nm.

For bio-optical research, tissue phantoms have been routinely used as the platform of study during the past decades. In contrast to the complexity and unpredictability of biotissues (e.g., optical properties of real tissues usually are heterogeneous), tissue phantoms are controllable, stable, and repeatable. Such characteristics have made them very popular among the bio-optics and bio-photonics research community, particularly for preliminary or early-staged researches. For example, Hull et al. [34], and Ramanujam et al. [35, 36], respectively, have used optical tissue phantoms as the study platform for their (respective) researches on the fluorescence spectroscopy, Sokolov et al. have used tissue phantoms for their research on the reflectance spectroscopy [37, 38], Gossage et al. [39] have used tissue phantoms for their work on the optical coherence tomography, and so on.

To construct tissue phantoms, both inorganic and organic materials, individually or in combination, could be used to achieve the desired optical properties, or to mimic optical properties of specific biology tissues. Inorganic materials, including polystyrene microspheres [40], India ink [36], intralipid [41], and aluminum oxide [42] all have been used to construct tissue phantoms. Particularly, polystyrene microspheres were mainly used for their scattering perspectives while India ink was mainly used for its absorption perspective. As for organic materials, it has been reported that collagen-based gels, which were derived from the tendon of rat tails [38, 39], were used to construct tissue phantoms for optical research.

For the nanoshell-assisted optical research, unique advantages of using phantoms are that nanoshells could be embedded within homogeneously, and nanoshell concentration are readily controllable as well. For in vivo experiments, which should be performed when the nanoshell-assisted diagnostic imaging research comes to a more mature stage, different mechanisms potentially would induce nanoshells to bypass healthy tissues and preferentially accumulate on the cancerous tissue site. The most fundamental mechanism is passive accumulation, caused by enhanced permeability and retention effect (ERP). The phenomenon of ERP was recognized for the first time by Maeda in 1986 [49] and ever since then has been studied extensively [50–53].

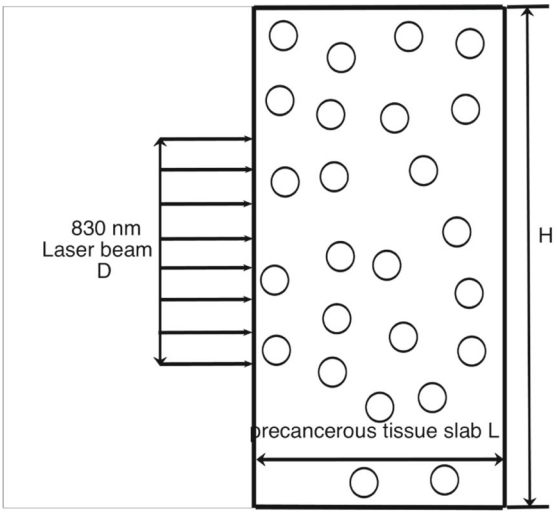

(a) single-layer model

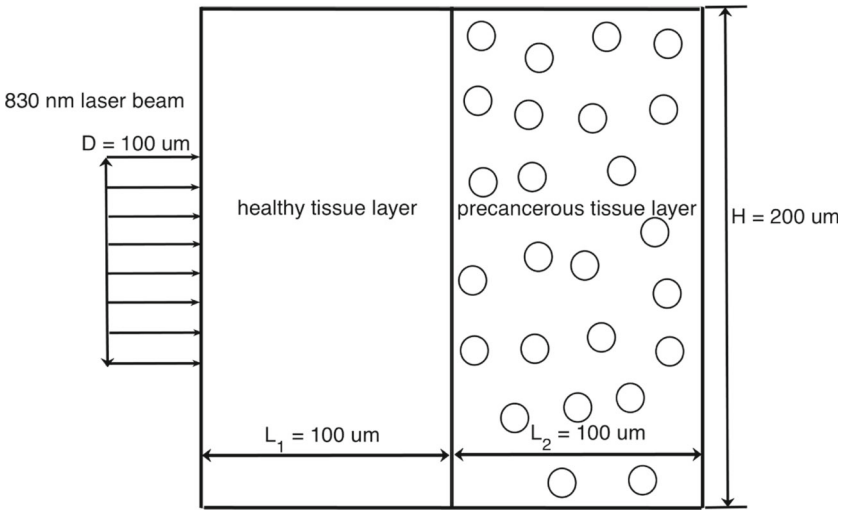

(b) dual-layer tissue model

Fig. 1 Platform of parametric study, illustration of **a** single-layer planar tissue model **b** dual-layer planar tissue model

The references [43–45, 48] have been consulted for optical properties of healthy and cancerous tissues for the NIR spectrum. The single-layer phantom model fundamentally mimics a slab of tissue in metastatic state. Prior to embedding nanoshells to the phantom, optical properties of which are such that $k_{\alpha,t} = 0.005$ mm^{-1}, $k_{s,t} = 2$ mm^{-1} and $g = 0.92$. After nanoshells of different generics being embedded, optical properties of the phantom should be overall parameters that take both hosting tissue and hosted nanoshells into account, i.e., $k_\alpha = k_{\alpha,t} + k_{\alpha,exo}$ and $k_s = k_{s,t} + k_{s,exo}$. The dual-layer phantom model has taken the fact that metastatic tissues are usually enclosed by healthy tissues into consideration. As Fig. 1b illustrates, the (assumed) healthy tissue layer is exposed directly to laser irradiance while the (assumed) metastatic tissue layer hides behind. Nanoshells are embedded in the metastatic tissue only. Optical properties for the healthy tissue are set such that $k_{\alpha,t} = 0.15$ mm^{-1}, $k_s = 2$ mm^{-1} and $g = 0.92$. (In vivo tissue sample examined for different NIR wavelengths have revealed that normal tissues almost always have a higher absorption coefficient than the same tissue in the metastases state.)

The R[50, 10], R[40, 15], R[55, 25], R[40, 40], R[75, 40], R[104, 23] and R[154, 24] nanoshells would be tested as the exogenous contrast agent, among which, the R[50, 10] and R[40, 15] nanoshells are preferentially absorbing while

Table 1 Optical properties of different nanoshell generics under the wavelength of 830 nm (C_s: scattering cross section, C_α: absorption cross section, Q_s: scattering efficiency, Q_α: absorption efficiency, g: anisotropy factor, ω: scattering albedo)

Nanoshell	ω	Q_s	Q_α	$C_s(\text{mm}^2)$	$C_\alpha(\text{mm}^2)$	g
R[50, 10]	0.2748	1.11	2.93	8.7135E-9	2.3000E-8	N/A
R[40, 15]	0.4122	1.08	1.54	5.4259E-9	7.7370E-9	N/A
R[55, 25]	0.7613	3.38	1.06	3.2105E-8	1.0068E-8	N/A
R[40, 40]	0.8633	3.22	0.51	1.6177E-8	2.5622E-9	N/A
R[75, 40]	0.9000	3.33	0.37	5.8816E-8	6.5351E-9	N/A
R[104, 23]	0.7690	2.83	0.85	9.6113E-8	2.8868E-8	0.148
R[154, 24]	0.7574	3.09	0.99	2.3011E-7	7.3724E-8	0.457

the rest five generics are all preferentially scattering. For the wavelength of 830 nm, Q_α, Q_s and g of these nanoshell generics are presented in Table 1. The raw data were firstly published by Lin [31]. Following Eq. 3, C_α and C_s have been computed and the results are presented in Table 1 as well.

The nanoshell volume fraction V_f has been introduced to quantify the nanoshell accumulation/retention in the target tissue site, which not only takes into consideration the number of nanoshells residing in the tissue but also the volume of a single nanoshell particle:

$$V_f = \frac{\text{volume of hosted nanoshells}}{\text{volume of hosting tissues}} \tag{10}$$

Following arguments of Lin on possible range of nanoshell retention rate in turbid medium [31], V_f has sequentially been set to $4.20e-6$, $6.56e-5$, and $5.25e-4$, to represent a gradually increasing nanoshell density in the tissue. For each value of V_f, the corresponding value for N_T has been calculated for each nanoshell generic and the results are listed in Table 2. Further, $k_{\alpha,exo}$ and $k_{s,exo}$ for each nanoshell generic are computed following Eq. 3 and the results are listed in Table 2 as well. (Note: For the rest of this paper, the diffuse reflectance presented is the normalized diffuse reflectance, the normalization is against q_0, the magnitude of the laser irradiance.)

Single-layer tissue model

The single-layer model would be investigated in this subsection. As Fig. 1a illustrates, nanoshell embedded cancerous tissue is directly exposed to the laser irradiance. Thickness of the tissue slab L is 100 μm, height of which H is 200 μm, width of the irradiating laser beam is 100 μm, which is half of H. How the diffuse reflectance signal is affected by the nanoshell generic, the nanoshell accumulation density, the laser irradiance and the thickness of tissue slab would be systematically investigated.

Table 2 Absorption and scattering coefficients $k_{\alpha,exo}$ and $k_{s,exo}$ for different nanoshells generics under different values of nanoshell volume fraction V_f

Nanoshell	N_T (mm^{-3})	$k_{s,exo}(\text{mm}^{-1})$	$k_{\alpha,exo}(\text{mm}^{-1})$
$V_f = 4.20\text{e-}6$			
R[50, 10]	4.629E6	0.040	0.106
R[40, 15]	6.011E6	0.033	0.047
R[55, 25]	1.953E6	0.063	0.019
R[40, 40]	1.953E6	0.032	0.005
R[75, 40]	6.575E5	0.039	0.004
R[104, 23]	4.882E5	0.047	0.014
R[154, 24]	1.773E5	0.041	0.013
$V_f = 6.56\text{e-}5$			
R[50, 10]	7.234E7	0.630	1.663
R[40, 15]	9.391E7	0.509	0.727
R[55, 25]	3.052E7	0.979	0.307
R[40, 40]	3.052E7	0.493	0.078
R[75, 40]	1.027E7	0.604	0.067
R[104, 23]	7.628E6	0.733	0.220
R[154, 24]	2.771E6	0.637	0.204
$V_f = 5.25\text{e-}4$			
R[50, 10]	5.787E8	5.043	13.310
R[40, 15]	7.513E8	4.077	5.813
R[55, 25]	2.441E8	7.838	2.458
R[40, 40]	2.441E8	3.949	0.626
R[75, 40]	8.219E7	4.834	0.537
R[104, 23]	6.102E7	5.865	1.762
R[154, 24]	2.216E7	5.100	1.634

Influences of nanoshell generics and accumulation rate on the diffuse reflectance

How the diffuse reflectance is affected by optical properties and target-specific accumulation of nanoshells is investigated in this sub-subsection. For experimental practices, the diffuse reflectance signal is collected by placing fiber-optic based spectrometers at different positions along the boundary [1, 2]. Being consistent with experimental practice, the diffuse reflectance along left boundary of the tissue slab, without and with nanoshells embedded, is computed and the results are presented as Fig. 2 with Fig. 2a, b and c corresponding to $V_f = 4.20e-6$, $V_f = 6.56e-5$ and $V_f = 5.25e-4$ respectively. The $x-$ axis corresponds to the normalized distance x/L and the $y-$ axis corresponds to the diffuse reflectance. As Fig. 1 illustrates, the incoming laser irradiance is for $x/L \in [0.25, 0.75]$. The black dash-dot curves in Fig. 2a–c correspond to the situation that no nanoshells of any generic are embedded in the tissue. Solid lines of different colors correspond to situations that different nanoshell generics are embedded in the tissue slab.

Figure 2a shows that for $V_f = 4.20e-6$, without and with nanoshells embedded, the diffuse reflectance signal doesn't change much. This implies that the corresponding nanoshell accumulation in the tissue slab is not sufficiently enough for nanoshells to take effect. When V_f is increased to $6.56e-5$ (Fig. 2b) and further to $5.25e-4$ (Fig. 2c), the embedded nanoshells do change the diffuse reflectance appreciably. For the same nanoshell generic, the bigger the nanoshell volume fraction V_f is, the more alternations in the diffuse reflectance signal. Figure 2b and c show that the diffuse reflectance signal has been enhanced by every nanoshell generic, including the preferentially absorbing $R[40, 15]$ and $R[50, 10]$ nanoshells. For the same V_f, the $R[55, 25]$ nanoshell enhances the diffuse reflectance signal the most while the $R[50, 10]$ nanoshell enhances it the least. If we rank the seven nanoshell generics according to their capacity of promoting the diffuse reflectance signal, the order would be: $R[55, 25]$ (which enhances the signal the most), $R[104, 23]$, $R[75, 40]$, $R[154, 24]$, $R[40, 40]$, $R[40, 15]$ and $R[50, 10]$ (which enhances the signal the least). It is also noted that for $V_f = 6.56e-5$, diffuse reflectance curves corresponding to the $R[75, 40]$ and $R[154, 24]$ nanoshells almost overlap with each other. This implies that the two nanoshell generics affect the diffuse reflectance signal in a similar way, despite of the fact that Q_α for the $R[154, 24]$ nanoshell is almost three times that of the $R[75, 40]$ nanoshell.

Peaks of diffuse reflectance curves in Fig. 2b and c are listed under the "Peak" column in Table 3. The percentage of alternation in diffuse reflectance peak induced by nanoshells has been computed following the below formula and the results are presented under the "Diff(%)" column in the table:

$$Diff = \frac{\text{peak with nanoshells embedded in the slab - peak without nanoshells embedded in the slab}}{\text{peak without nanoshells embedded in the slab}} \times 100\% \quad (11)$$

The capacity of enhancing the diffuse reflectance signal of different nanoshell generics has been ranked and the results are listed under the "rank" column of the table. It is seen that the top three nanoshells that promote the diffuse reflectance signal the most are the $R[55, 25]$, $R[104, 23]$, and $R[75, 40]$ nanoshells, which have respectively promoted the diffuse reflectance peak by 51.39%, 38.44% and 33.49%, for $V_f = 6.56e-5$. After the nanoshell volume fraction V_f is increased to $5.25e-4$, the same three nanoshells have respectively promoted the diffuse reflectance peak by 590.88%, 367.71%, and 383.09% (in other words, the diffuse reflectance peak has been enhanced by a factor of ~ 5.9, ~ 3.8, and ~ 3.7).

Influences of laser irradiance on the diffuse reflectance

How diffuse reflectance is affected by the irradiating laser beam is investigated in this sub-subsection. The width of laser beam is increased from 100 μm, half of the tissue slab height, to 200 μm, height of the tissue slab. All the other conditions are the same as what have been presented in "Influences of nanoshell generics and accumulation rate on the diffuse reflectance." Without and with nanoshell embedded, the diffuse reflectance along left boundary of the slab has been computed and the results are presented as Fig. 3. Figure 3a, b, and c corresponds to $V_f = 4.20e-6$, $V_f = 6.56e-5$, and $V_f = 5.25e-4$ respectively. Peaks of diffuse reflectance curves in Fig. 3b and c are listed in Table 4 (see the "Peak" column). The alternation in diffuse reflectance peak induced by nanoshells has been calculated following Eq. 11 and the results are presented in Table 4 as well. The capacity of enhancing the diffuse reflectance signal of different nanoshell generics has been ranked and the results are presented under the "Rank" column.

If compare Fig. 2 against Fig. 3, it could be seen that for the same V_f and nanoshell generic, the wider the laser beam is, the more the diffuse reflectance signal would be altered by nanoshells. For example, for $V_f = 5.25e-4$, the three nanoshell generics that enhance the diffuse reflectance signal the most, namely, the $R[55, 25]$, $R[104, 23]$ and $R[75, 40]$ nanoshells, have respectively promoted the diffuse reflectance peak by a factor of ~ 5.9, ~ 3.8, and ~ 3.7 when the laser beam is of a width of 100 μm (see Table 3). After the width of the laser beam being doubled, for the same V_f, the same three nanoshells have respectively promoted the diffuse reflectance peak by a factor of ~ 6.3, ~ 4.0 and ~ 3.9 (see Table 4).

Figure 3 also shows that for $V_f = 6.56e-5$, diffuse reflectance curves for the $R[75, 40]$ and $R[154, 24]$ nanoshells almost overlap with each other while for $V_f = 5.25e-4$, diffuse reflectance curves for the $R[104, 23]$ and $R[75, 40]$ nanoshells almost overlap with each other, which confirms the conclusion drawn in "Influences of nanoshell generics and accumulation rate on the diffuse reflectance" that the diffuse reflectance signal might be affected in a similar way by different nanoshell generics, even though optical properties of the nanoshells are quite different.

Influences of thickness of tissue slab on the diffuse reflectance

How the diffuse reflectance is affected by the thickness of the tissue slab is investigated in this sub-subsection. The

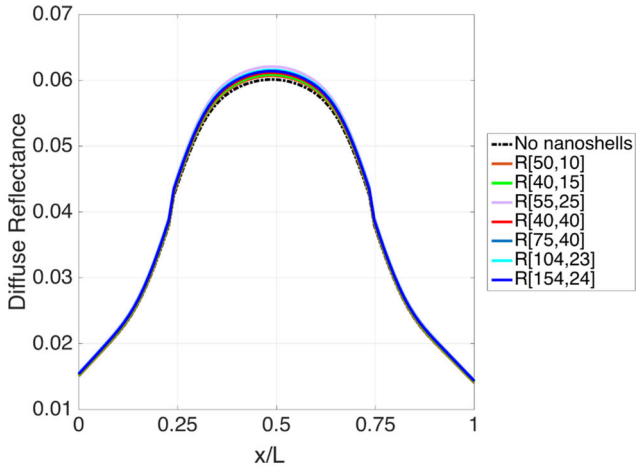

(a) $V_f = 4.20e-6$

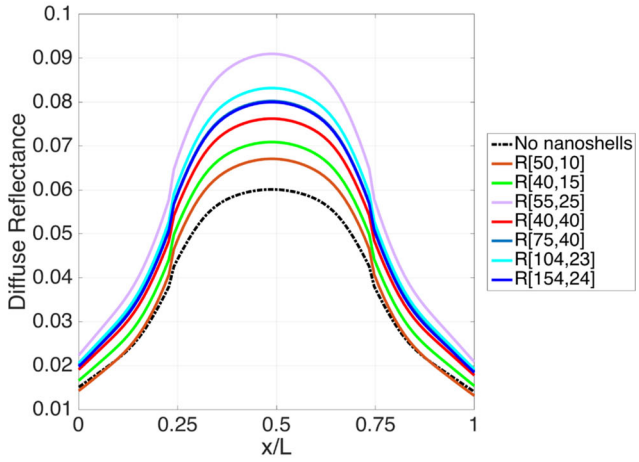

(b) $V_f = 6.56e-5$

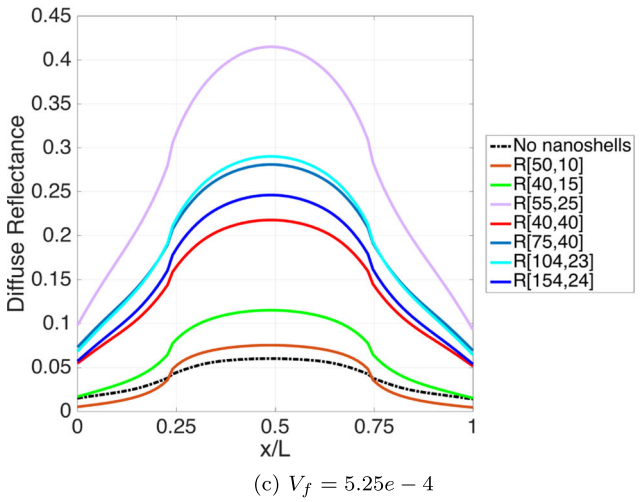

(c) $V_f = 5.25e-4$

Fig. 2 Single-layer model: distribution of the diffuse reflectance along left boundary of the slab when different nanoshells generics embedded as the exogenous contrast agent (thickness of the tissue slab $L = 100\ \mu$m, height of the tissue slab $H = 200\ \mu$m and width of the laser beam $D = 100\ \mu$m)

Table 3 Single-layer model: peak and minimum of the diffuse reflectance along left boundary of the slab, with and without nanoshells embedded (thickness of the slab $L = 100$ um, height of the slab $H = 200$ um and width of the laser beam $D = 100$ um

	$V_f = 6.56e-5$			$V_f = 5.25e-4$		
Nanoshell	Peak	Diff (%)	Rank	Peak	Diff(%)	Rank
w/o	0.0601			0.0601		
R[50,10]	0.0671	11.59	7	0.0754	25.38	7
R[40,15]	0.0709	17.96	6	0.1152	91.73	6
R[*55,25*]	*0.0910*	*51.39*	*1*	*0.4152*	*590.88*	*1*
R[40,40]	0.0762	26.82	5	0.2180	262.70	5
R[*75,40*]	*0.0802*	*33.49*	*3*	*0.2811*	*367.71*	*3*
R[*104,23*]	*0.0832*	*38.44*	*2*	*0.2903*	*383.09*	*2*
R[154,24]	0.0780	33.11	4	0.2463	309.89	4

thickness of the tissue slab increases from 100 μm to 200 μm while all the other conditions are the same as what have been presented in "Influences of nanoshell generics and accumulation rate on the diffuse reflectance." Without and with nanoshell embedded, the diffuse reflectance along left boundary of the slab has been computed and the results are presented as Fig. 4. Figure 4a, b, and c correspond to $V_f = 4.20e-6$, $V_f = 6.56e-5$, and $V_f = 5.25e-4$ respectively. Peaks of diffuse reflectance curves in Fig. 4b and c are listed in Table 5 (see the "Peak" column). The alternation in the diffuse reflectance peak induced by nanoshells has been calculated following Eq. 11 and the results are presented under the "Diff(%)" column. The capacity of enhancing the diffuse reflectance signal of different nanoshell generics have been ranked and the results are presented under the "Rank" column in the table as well.

If compared Fig. 2 against Fig. 4, it could be seen that for the same V_f and nanoshell generic, the thicker the tissue slab is, the more the diffuse reflectance signal would be altered by the nanoshells, particularly if V_f is high. For example, for $V_f = 5.25e-4$, the *R*[55, 25], *R*[75, 40] and *R*[104, 23] nanoshells have respectively enhanced the diffuse reflectance peak by a factor of ~ 5.9, ~ 3.7 and ~ 3.8 when thickness of the tissue slab is 100 μm (see Table 3). When thickness of the tissue slab is 200 μm, the same three nanoshell generics have respectively promoted the diffuse reflectance peak by a factor of ~ 18.9, ~ 6.6, and ~ 5.9 (see Table 5). Such dramatic increase in the influence of nanoshells on the diffuse reflectance signal could partially be explained by the fact that for the same V_f, when thickness of the tissue slab increases, the number of nanoshells embedded in the tissue slab increases as well. Therefore, interactions among laser photons, nanoshells and the hosting tissue are much more intensive, which are displayed as bigger alterations in the diffuse reflectance signal macroscopically.

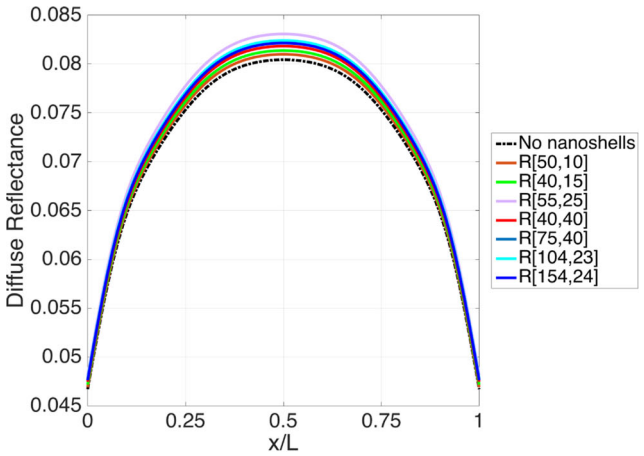

(a) $V_f = 4.20e-6$

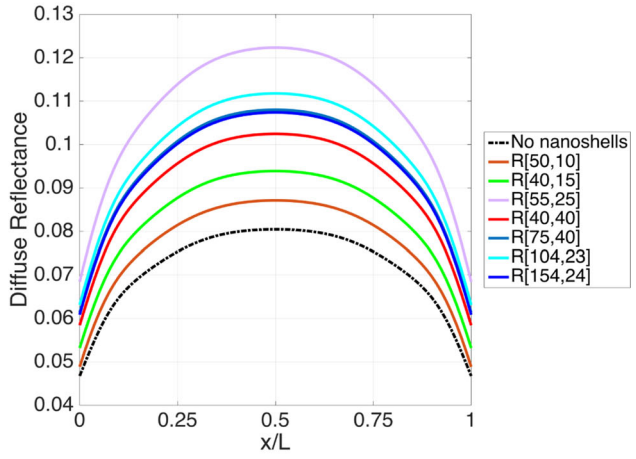

(b) $V_f = 6.56e-5$

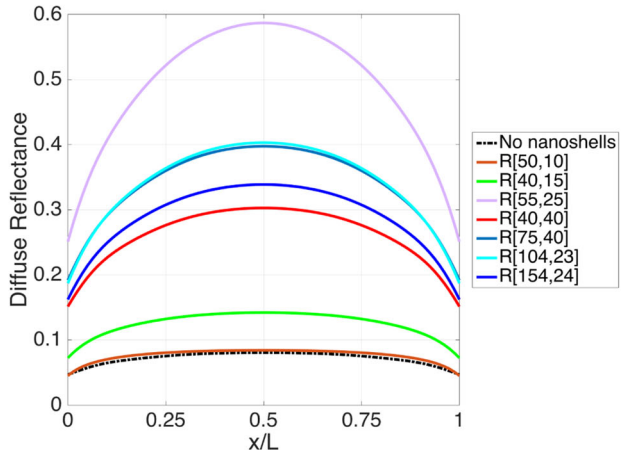

(c) $V_f = 5.25e-4$

Fig. 3 Single-layer model: distribution of the diffuse reflectance along left boundary of the slab when different nanoshell generics are embedded as the exogenous contrast agent (thickness of the slab $L = 100\ \mu$m, height of the slab $H = 200\ \mu$m and width of the laser beam $D = 200\ \mu$m)

Table 4 Single-layer model: peak and minimum of the diffuse reflectance along left boundary of the slab, with and without nanoshells embedded (thickness of the slab $L = 100$ um, height of the slab $H = 200$ um and width of the laser beam $D = 200$ um

	$V_f = 6.56e-5$			$V_f = 5.25e-4$		
Nanoshell	Peak	Diff(%)	Rank	Peak	Diff(%)	Rank
w/o	0.0804			0.0804		
R[50,10]	0.0871	8.27	7	0.0841	4.56	7
R[40,15]	0.0938	16.68	6	0.1420	76.59	6
R[55,25]	*0.1223*	*52.04*	*1*	*0.5870*	*629.76*	*1*
R[40,40]	0.1024	27.32	5	0.3027	276.35	5
R[75,40]	*0.1080*	*34.23*	*3*	*0.3976*	*394.26*	*3*
R[104,23]	*0.1117*	*38.91*	*2*	*0.4031*	*401.10*	*2*
R[154,24]	0.1074	33.46	4	0.3387	321.15	4

It is also noticed that for $V_f = 5.25e-4$, after thickness of the tissue slab increases from 100 μm to 200 μm, the *R*[75, 40] nanoshell has replaced the *R*[104, 23] nanoshell as the second-place nanoshell generic that enhance the diffuse reflectance signal the most. Besides, when thickness of the tissue slab is 200 μm, the *R*[50, 10] nanoshell diminishes the diffuse reflectance signal instead of enhancing it as it does when thickness of the tissue slab is 100 μm (According to Table 5, decrement in the diffuse reflectance peak is 46.38% and 11.71% respectively for $V_f = 6.56e-5$ and $V_f = 5.25e-4$). Such observations indicate that dependences of the diffuse reflectance signal on the irradiating lights, hosting tissue and hosted nanoshells are highly nonlinear and should be handled case by case. Generalization might be problematic.

Dual-layer tissue model

Taking the fact that cancerous tissues are usually enclosed by healthy tissue into consideration, a dual-layer model, illustrated as Fig. 1b, would be investigated in this subsection. As Fig. 1b shows, laser lights have to transverse the healthy tissue to reach the cancerous tissue. Nanoshells are confined within the cancerous tissue only. Thickness for both healthy and cancerous tissues is 100 μm. Height of the tissue slab again is 200 μm. Width of the laser beam is 100 μm, which is half of the tissue slab height.

Without and with nanoshells embedded in the cancerous tissue, diffuse reflectance along left boundary of the slab has been computed and the results are presented as Fig. 5. Figure 5a, b, and c corresponds to $V_f = 4.20e-6$, $V_f = 6.56e-5$ and $V_f = 5.25e-4$ respectively. Peaks of diffuse reflectance curves in Fig. 5b and c are listed under the "Peak" column in Table 6. The alternation in diffuse reflectance peak induced by nanoshells has been calculated following Eq. 11 and the results are presented under

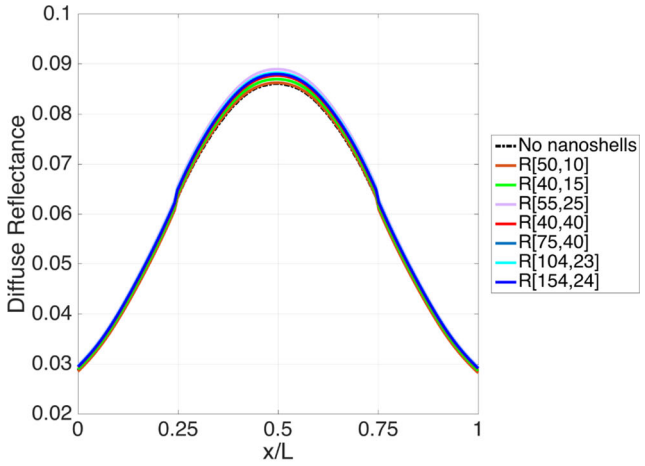

(a) $V_f = 4.20e-6$

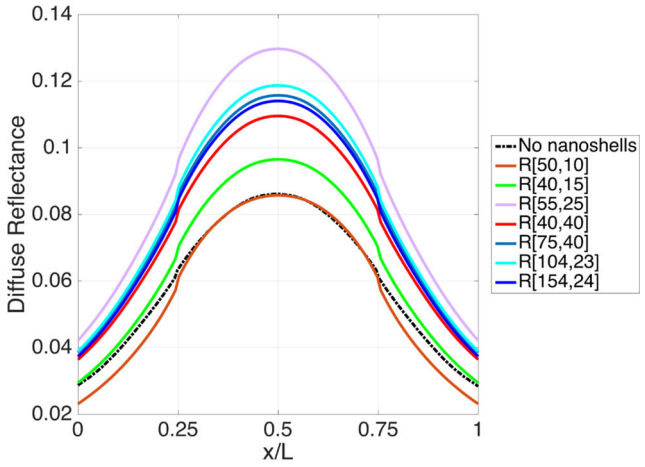

(b) $V_f = 6.56e-5$

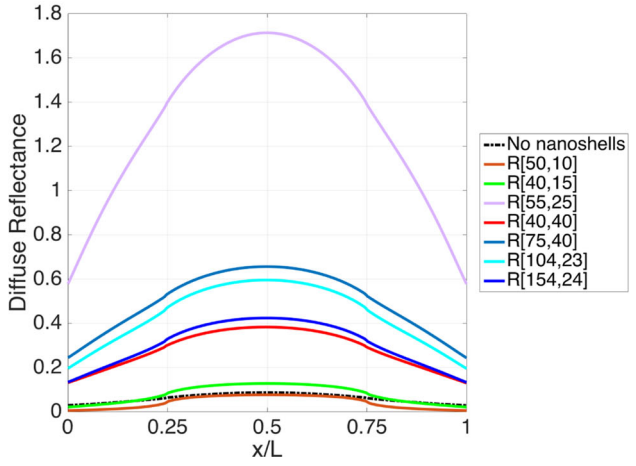

(c) $V_f = 5.25e-4$

Fig. 4 Single-layer model: distribution of the diffuse reflectance along left boundary of the slab when different nanoshell generics are embedded as the exogenous contrast agent (thickness of the slab $L = 200\ \mu$m, height of the slab $H = 200\ \mu$m and width of the laser beam $D = 100\ \mu$m)

Table 5 Single-layer model: peak and minimum of the diffuse reflectance along left boundary of the slab, with and without nanoshells embedded (thickness of the slab $L = 200$ um, height of the slab $H = 200$ um and width of the laser beam $D = 100$ um

	$V_f = 6.56e-5$			$V_f = 5.25e-4$		
Nanoshell	Peak	Diff(%)	Rank	Peak	Diff(%)	Rank
w/o	0.0862			0.0862		
R[50, 10]	0.0462	− 46.38	7	0.0761	− 11.71	7
R[40, 15]	0.0965	11.95	6	0.1272	47.63	6
R[55, 25]	*0.1296*	*50.45*	*1*	*1.7130*	*1887.94*	*1*
R[40, 40]	0.1095	27.08	5	0.3824	343.81	5
R[75, 40]	*0.1157*	*34.26*	*3*	*0.6559*	*661.21*	2
R[104, 23]	*0.1187*	*37.73*	*2*	*0.5950*	*590.54*	*3*
R[154, 24]	0.1140	32.31	4	0.4234	391.37	4

the "Diff(%)" column. The capacity of enhancing the diffuse reflectance signal of different nanoshell generics have been ranked and the results are presented under the "rank" column in Table 6 as well.

If compare Fig. 2 against Fig. 5, it could be seen that for the same V_f and nanoshell generic, alterations in the diffuse reflectance signal induced by nanoshells are not as significant for the dual-layer model as what has been for the single-layer model. For example, for $V_f = 5.25e-4$, under the dual-layer model, the top three nanoshells that promotes the diffuse reflectance signal the most, namely the $R[55, 25]$, $R[75, 40]$ and $R[104, 23]$ nanoshells have respectively promoted the diffuse reflectance peak by 83.64%, 75.27%, and 60.31%. Although such enhancement in the diffuse reflectance is very impressive already, it is not comparable to what have been displayed under the single-layer model.

Figure 5a shows that for $V_f = 4.20e-6$, all the diffuse reflectance curves cluster, which implies that nanoshell accumulation corresponding to this value of V_f is not sufficiently enough for nanoshells to take effect. Such observation is consistent with what has been observed from the single-layer model. For $V_f = 6.56e-5$, the preferentially absorbing $R[50, 10]$ nanoshell diminishes the diffuse reflectance signal instead of enhancing it. For $V_f = 5.25e-4$, the preferentially absorbing $R[50, 10]$ and $R[40, 15]$ nanoshells both diminish the diffuse reflectance signal. Such observation is different from what has been observed from the single-layer model, for which all seven nanoshell generics enhance the diffuse reflectance.

Influence of absorption perspective of nanoshells on the diffuse reflectance

For the scattering-based diagnostic imaging, whether it is well justified to neglect the absorption characteristic of the

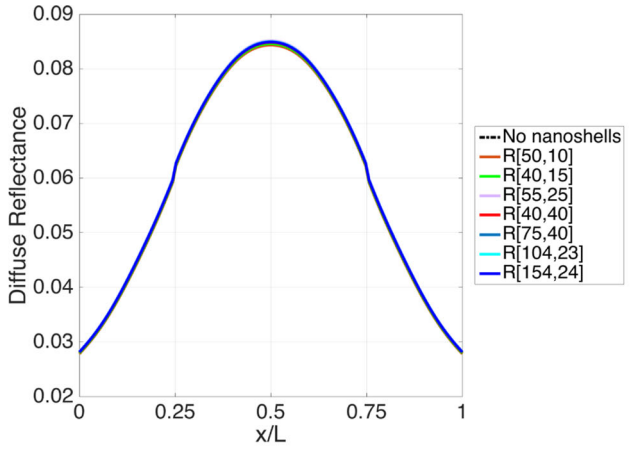

(a) $V_f = 4.20e-6$

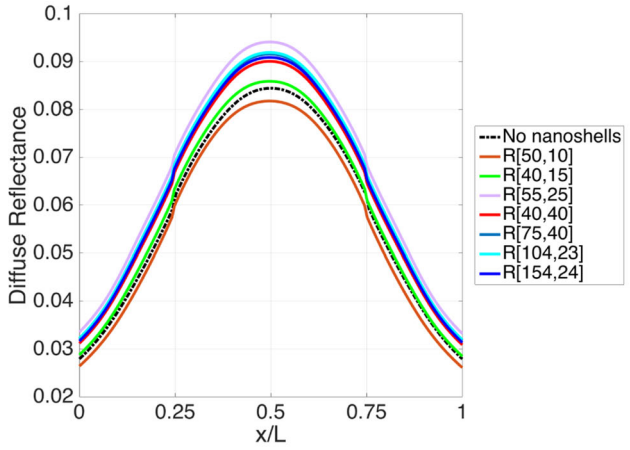

(b) $V_f = 6.56e-5$

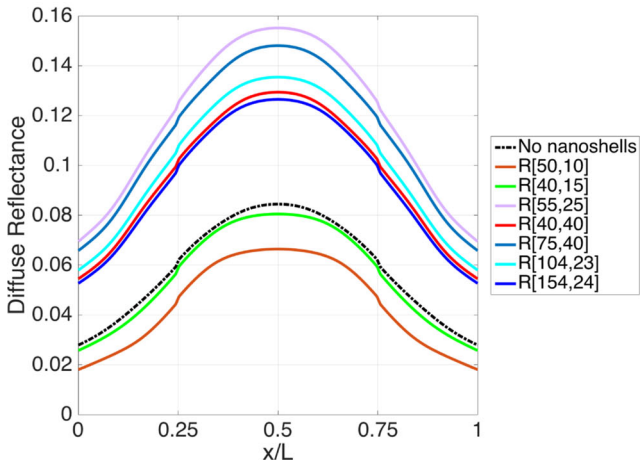

(c) $V_f = 5.25e-4$

Fig. 5 Dual-layer model: distribution of the diffuse reflectance along left boundary of the slab when different nanoshell generics are embedded as the exogenous contrast agent (thickness of the healthy tissue layer $L_1 = 100\ \mu m$, thicknesses of the cancerous tissue layer $L_2 = 100\ \mu m$, height of the slab $H = 200\ \mu m$ and width of the laser beam $D = 100\ \mu m$)

Table 6 Dual-layer model: peak and minimum of the diffuse reflectance along left boundary of the slab, with and without nanoshells embedded (thickness of the slab $L = 200\ \mu$m, height of the slab $H = 200\ \mu$m and width of the laser beam $D = 100\ \mu$m)

	$V_f = 6.56e-5$			$V_f = 5.25e-4$		
Nanoshell w/o	Peak 0.0845	Diff (%)	Rank	Peak 0.0845	Diff (%)	Rank
R[50,10]	0.0818	− 3.15	7	0.0664	− 21.38	7
R[40,15]	0.0859	1.70	6	0.0805	− 4.69	6
R[*55,25*]	*0.0942*	*11.53*	*1*	*0.1551*	*83.64*	*1*
R[40,40]	0.0901	6.68	5	0.1265	49.77	5
R[*75,40*]	*0.0916*	*8.28*	*3*	*0.1481*	*75.27*	*2*
R[*104,23*]	*0.0919*	*8.76*	*2*	*0.1354*	*60.31*	*3*
R[154,24]	0.0909	7.62	4	0.1294	53.21	4

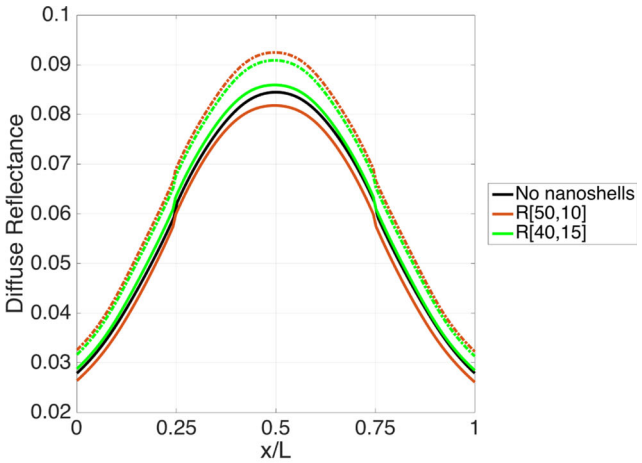

(a) Preferentially absorbing nanoshells

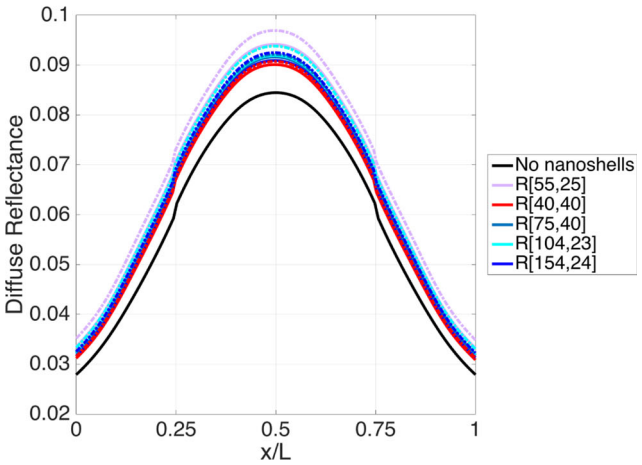

(b) Preferentially scattering nanoshells

Fig. 6 Dual-layer model: distribution of the diffuse reflectance along left boundary of the slab with and without considering the absorption perspective of the nanoshells, $V_f = 6.56$e-5 (*dot-dashed lines*: results generated by neglecting the absorption perspective of nanoshells; *solid lines*: results generated by taking both absorption and scattering perspectives of nanoshells into account; *black solid lines*: results when no nanoshells of any generic are embedded in the cancerous tissue)

exogenous contrast agent would be investigated in this subsection. The dual-layer model, as Fig. 1b illustrates, is used as the platform for study. The seven nanoshell generics are classified into two groups: nanoshells that are preferentially absorbing (the $R[50, 10]$ and $R[40, 15]$ nanoshells fall into this category) and nanoshells that are preferentially scattering (the $R[55, 25]$, $R[40, 40]$, $R[75, 40]$, $R[104, 23]$, and $R[154, 24]$ nanoshells fall into this category). The diffuse reflectance along left boundary of the slab has been computed and the results are presented as Fig. 6 (for $V_f = 6.56e - 5$) and Fig. 7 (for $V_f = 5.25e - 4$). Figures 6a and 7a are for nanoshells that are preferentially absorbing, presenting comparisons of the diffuse reflectance signal with and without the absorption perspective of the nanoshells being taken into account. Similarly, Fig. 6b and 7b are for nanoshells that are preferentially scattering.

Peak and minimum of diffuse reflectance curves in Figs. 6 and 7 have been listed in Table 7. The percentage of differences in peak and minimum of diffuse reflectance with and without taking nanoshell's absorption into account, has been calculated following the formula below and the resulted are presented under the "Diff(%)" column in the table as well:

$$Diff = \frac{\text{peak/minimum when } k_{\alpha,exo} \text{ is not counted - peak/minimum when } k_{\alpha,exo} \text{ is counted}}{\text{peak/minimum when } k_{\alpha,exo} \text{ is counted}} \times 100\% \quad (12)$$

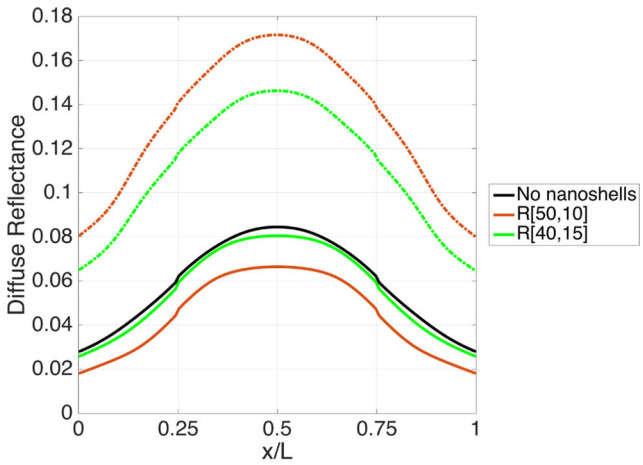

(a) Preferentially absorbing nanoshells

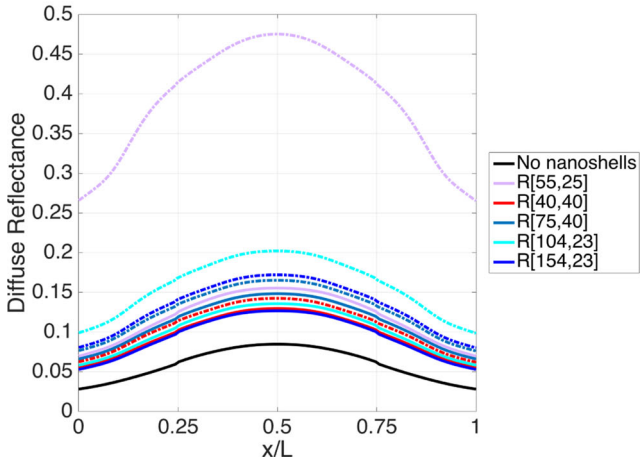

(b) Preferentially scattering nanoshells

Fig. 7 Dual-layer model: distribution of the diffuse reflectance along left boundary of the slab with and without considering the absorption perspective of the nanoshells, $V_f = 5.25\text{e}{-4}$ (*dot-dashed lines*: results generated by neglecting the absorption perspective of nanoshells; *solid lines*: results generated by taking both absorption and scattering perspectives of nanoshells into account; *black solid lines*: results when no nanoshells of any generic are embedded in the cancerous tissue)

Figure 6 demonstrates that for $V_f = 5.65e - 5$ and for the preferentially absorbing $R[50, 10]$ and $R[40, 15]$ nanoshells, neglecting the particle's absorption leads to an over-prediction of the diffuse reflectance signal. For the preferentially scattering $R[55, 25]$, $R[40, 40]$, $R[75, 40]$, $R[104, 23]$, $R[154, 24]$ nanoshells, whether the particle's absorption being taken into account or not doesn't seem to affect the diffuse reflectance signal much. Figure 7 demonstrates that for $V_f = 5.25e-4$, regardless of whether the nanoshell is preferentially absorbing or preferentially scattering, neglecting the particle's absorption leads to serious over-predictions of the diffuse reflectance signal. According to Table 7, for $V_f = 5.25e - 4$ and for the three nanoshells that enhance the diffuse reflectance signal the most, i.e., the $R[55, 25]$, $R[75, 40]$ and $R[104, 23]$ nanoshells, without taking nanoshell's absorption into account, peak of the diffuse reflectance has respectively been overly predicted by 206.23%, 49.11%, and 11.46% while minimum of the diffuse reflectance has respectively been overly predicted by 281.50%, 69.58%, and 15.41%.

It is therefore concluded that within the context of scattering-based optical imaging, although the practice of neglecting the absorption of the exogenous contrast agent is quite common among the bio-nano community, such practice is by no means well justified. It might lead to unrealistic faiths in the emerging nanoparticle assisted diagnostic imaging and if not handled properly, this could be a pitfall for this developing technique.

Conclusive remarks

Within the context of nanoparticle-assisted optical imaging for cancer detection, this work has performed systematical numerical parametric study to investigate the nonlinear dependence of diffuse reflectance on the laser irradiance, the hosting biology tissue, and the gold-silica nanoshells

Table 7 Peak and minimum of the diffuse reflectance curve with and without taking the absorption perspective of nanoshells into account

	Peak			Min		
Nanoshell	w/o abs	with abs	Diff (%)	w/o abs	with abs	Diff (%)
$V_f = 6.56e-5$						
$R[50, 10]$	0.0925	0.0818	13.07	0.0322	0.0261	23.62
$R[40, 15]$	0.0909	0.0859	5.77	0.0313	0.0285	9.99
$R[55, 25]$	0.0969	*0.0942*	*2.95*	*0.0348*	*0.0332*	*4.95*
$R[40, 40]$	0.0901	0.0624	1.23	0.0312	0.0309	1.24
$R[75, 40]$	*0.0921*	*0.0916*	*0.57*	0.0321	*0.0317*	*0.96*
$R[104, 23]$	*0.0938*	*0.0919*	*2.03*	0.0330	*0.0319*	*3.49*
$R[154, 24]$	0.0925	0.0909	1.74	0.0322	0.0313	2.92
$V_f = 5.25e-4$						
$R[50, 10]$	0.1716	0.0664	158.26	0.0799	0.0181	342.82
$R[40, 15]$	0.1463	0.0805	81.70	0.0645	0.0257	150.83
$R[55, 25]$	*0.4751*	*0.1551*	*206.23*	*0.2650*	*0.0695*	*281.50*
$R[40, 40]$	0.1422	0.1294	9.91	0.0618	0.0545	13.49
$R[75, 40]$	0.1650	0.1481	*11.46*	*0.0759*	*0.0658*	*15.41*
$R[104, 23]$	0.2019	*0.1354*	*49.11*	*0.0983*	*0.0580*	*69.58*
$R[154, 24]$	0.1718	0.1265	35.84	0.0799	0.0527	51.78

embedded as the exogenous contrast agent. Seven nanoshell generics, namely the $R[50, 10]$, $R[40, 15]$, $R[55, 25]$, $R[40, 40]$, $R[75, 40]$, $R[104, 23]$ and $R[154, 24]$ nanoshells have been tested. Basing on the study, the following conclusions have been drawn:

1. The threshold dosage for nanoshells to take effect as the exogenous contrast agent depends on many factors including those associated with hosting tissue and laser irradiance. Preliminary numerical investigations similar as this work, could provide a (rough) range for this threshold dosage. For real bench practice, such information could helps in cutting down unnecessary trials and shorten research cycles.
2. Judged by the capacity of enhancing the diffuse reflectance signal, among the seven nanoshell generics, the $R[55, 25]$ nanoshell seems to be the best candidate for exogenous contrast agent while the $R[75, 40]$ and $R[104, 23]$ nanoshells show good potentials as well. The preferentially absorbing $R[50, 10]$ and $R[40, 15]$ nanoshells should be avoided being used as exogenous contrast agent.
3. The practice of neglecting the absorption perspective of the exogenous contrast agent is not well justified. It is likely to end up with an over-prediction of the effectiveness and efficiency of the exogenous contrast agent, which probably will lead to false faith in the nanoparticle-assisted optical imaging.
4. Interactions among the laser light, the hosting tissue and the hosted nanoshells are highly nonlinear. Nanoshells with totally different optical properties might have have similar effects on the diffuse reflectance signal and vice versa. It is problematic to generalize. It is highly recommend that prior to any bench practice, some preliminary simulations are performed first to gain a preview of possible outcomes, according to which conditions of the the bench experiment could be adjusted so that an optimal outcome could be gained.

Compliance with Ethical Standards

Conflict of interest The author declare that there is no conflict of interest.

References

1. Liang C, Sung KB, Richards-Kortum RR, Descour MR (2002) Design of a high-numerical aperture minimature microscope objective for an endoscopic fiber confocal reflectance microscopy. Appl Optics 41(22):4603–4610
2. Sung KB, Liang C, Descour M, Collier T, Follen M, Richards-Kortum R (2002) Fiber-optic confocal reflectance microscope with miniature objective for in vivo imaging of human tissue. IEEE T Biomedi Eng 49(10):1168–1172
3. Barton JK, Halas NJ, West JL, Drezek RA (2004) Nanoshells as an optical coherence tomography contrast agent. Proc SPIE 5316: 99–106
4. Tucker-Schwartz JM, Meyer TA, Patil CA, Duvall CL, Skala MC (2012) In vivo photothermal optical coherence tomography of gold nanorod contrast agents. Biomed Opt Express 3(11):2882–2895
5. Kirillin MY, Agrba PD, Sirotkina MA, Shirmanova MV, Zagainova EV, Kamensky VA (2010) Nanoparticles as contrast-enhancing agents in optical coherence tomography imaging of

the structural components of skin: quantitative evaluation. Quant Electron 40(6):525–530
6. Zhou L, Wu G, Wei H, Guo Z, Yang H, He Y, Xie S, Liu Y, Meng Q (2015) Effects of titanium dioxide nanoparticles coupled with diode laser on optical properties of in vitro normal and cancerous human lung tissues studied with optical coherence tomography and diffuse reflectance spectra. J Biomed Opt 20(4):046003 (10pp)
7. Zhou F, Wei H, Ye X, Hu K, Wu G, Yang H, He Y, Xie S, Guo Z (2015) Influence of nanoparticles accumulation on optical properties of human normal and cancerous liver tissue in vitro estimated by OCT. Phys Med Biol 60:1385–1397
8. Krainov A, Mokeeva A, Sergeeva E, Zabotnov S, Kirillin M (2013) Nanoparticles as contrasting agents in diffuse optical spectroscopy. Proce SPIE 86990Q(8pp):8699
9. Zhang YQ, Wu GY, Wei HJ, Guo ZY, Yang HQ, He YH, Xie SS, Liu Y (2014) Effect of differently sized nanoparticles' accumulation on the optical properties of ex vivo normal and adenomatous human colon tissue with OCT imaging and diffuse reflectance spectra. Laser Phys Lett 085901(8pp):11
10. Lin A, Lewinski N, West J, Halas N, Drezek R (2005) Optically tunable nanoparticle contrast agents for early cancer detection: model-based analysis of gold nanoshells. J Biomed Opt 10(6):064035
11. Bayer CL, Kelvekar J, Emelianov SY (2013) Influence of nanosecond pulsed laser irradiance on the viability of nanoparticle-loaded cells: implications for safety of contrast-enhanced photo-acoustic imaging. Nanotechnology 24:465101 (8pp)
12. Fang W, Wei Y (2016) Upconversion nanoparticle as a theranostic agent for tumor imaging and therapy. J Innov Opt Health Sci 9(4):1630006(20pp)
13. Sajjadi AY, Suratkar A, Mitra K, Grace MS (2012) Short-pulse laser-based system for detection of tumors: administration of gold nanoparticles enhances contrast. J Nanotechnology Eng Med 3:021002 (6pp)
14. Hahn MA, Singh AK, Sharma P, Brown SC, Moudgil BM (2011) Nanoparticles as contrast agents for in-vivo bio-imaging: current status and future perspectives. Anal Bioanal Chem 399:3–27
15. Bardhan R, Grady NK, Cole JR, Joshi A, Halas NJ (2009) Fluorescene enhancement by Au nanostructures: nanoshells and nanorods. ACS Nano 3(3):744–752
16. Zagaynova EV, Shirmanova MV, Kirillin MY, Khlebtsov BN, Orlova AG, Balalaeva IV, Sirotkina MA, Bugrova ML, Agrba PD, Kamensky VA (2008) Contrasting properties of gold nanoparticles for optical coherence tomography: phantom, in vivo studies and Monte Carlo simulation. Phys Med Biol 53:4995–5009
17. Key J, Leary JF (2014) Nanoparticles for multimodal in vivo imaging in nanomedicine. Int J Nanomed 9:711–726
18. Shi Y, Fan S, Chen S, Jiang X, Zhao Q, Ren Q, Cui D, Zhou C (2014) OCT imaging enhancement of ovarian cancer using gold and gold/silver nanorods. Proc SPIE 9268:92682Q (7pp)
19. Zeng H, Petek M, Zorman MT, McWilliams A, Palcic B, Lam S (2004) Integrated endoscopy system for simultaneous imaging and spectroscopy for early lung cancer detection. Opt Lett 29(6):587–589
20. Onofre MA, Sopsto MR, Navarro CM (2001) Reliability of toluidine blue application in the detection of oral epithelial dysplasia and in situ and invasive squamous cell carcinomas, Oral Surg, Oral Med. Oral Path Oral Radi 91(5):535–540
21. Tincani AJ, Brandalise N, Altemani A, Scanavini RC, Valerio J, Lage HT, Molina G, Martins AS (2000) Diagnosis of superifical esophageal cancer and dysplasia using endoscopic screening with a 2% Lugol dye solution in patients with head and neck cancer. Head Neck 22(2):170–174
22. Xu X, Meade A, Bayazitoglu Y (2013) Feasibility of selctive nanoparticle-assisted photothermal treatment for an embedded liver tumor. Lasers Med Sci 28:1159–1168
23. Xu X, Meade A, Bayazitoglu Y (2011) Numerical investigation of nanoparticle-assisted laser-induced interstitial thermotherapy, toward tumor and cancer treatment. Lasers Med Sci 26:213–222
24. Xu X, Bayazitoglu Y, Meade A (2018) Evaluation of theranostic perspective of gold-silica nanoshell for cancers: a numerical parametric study. Lasers Med Sci under review
25. Vera J, Bayazitoglu Y (2009) Gold nanoshell density variation with laser power for induced hyperthermia. Int J Heat Mass Tran 52:564–573
26. Vera J, Bayazitoglu Y (2009) A note on laser penetration in nanoshell deposited tissue. Int J Heat Mass Tran 52(13/14):3402–3406
27. Eillot AM, Schwartz JS, Wang J, Shetty AM, Bougoyne C, O'Neal D, Hazle J, Stafford RJ (2009) Quantitative comparison of delta P1 versus optical diffusion approximations for modeling near-infrared gold nanoshell heating. Med Phys 36(4):1351–1358
28. Feng Y, Fuentes D, Hawkins A, Bass J, Rylander MN, Eillot A, Shetty A, Stafford RJ, Oden JT (2009) Nanoshell-mediated laser surgery simulation for prostate cancer treatment. Eng Comput 25:3–13
29. Xu X, Meade A, Bayazitoglu Y (2010) Fluence rate distribution in laser-induced interstitial thermotherapy by meshfree collocation. Int J Heat Mass Tran 53:4017–4022
30. Chai J, Lee H, Patankar S (1994) Finite volume method for radiative heat transfer. J Thermophys Heat Tran 8(3):419–425
31. Lin A (2006) Nanoengineered contrast agents for biophotonics: modeling and experimental measurements of gold nanoshell reflectance. Rice University, Ph.D dissertation
32. Henyey L, Greenstein J (1941) Diffuse radiation in the galaxy. Astrophys J 93:70–83
33. Mie G (1908) Beitrage zur Optik truber Medien, speziell kolloidaler metallosungen. Ann Phys 330:377–445
34. Hull E (1998) Nichols MG and Forster TH Quantitative broadband near-infrared spectroscopy of tissue-simulating phantoms containing erythrocytes. Phys Med Biol 43:3381–3404
35. Liu Q, Zhang C, Ramanujam N (2003) Experimental validation of Monte Carlo modeling of fluorescence in tissues in the UV-visible spectrum. J Biomed Opt 8(2):223–236
36. Liu Q, Ramanujam N (2004) Experimental proof of the feasibility of using an angled fiber-optic probe for depth-sensitive fluorescence spectroscopy of turbid media. Opt Lett 29(17):2034–2036
37. Sokolov K, Drezek R, Gossage K, Richards-Kortum R (1999) Reflectance spectroscopy with polarized light: is it sensitive to cellular and nuclear morphology. Opt Lett 5(13):302–317
38. Sokolov K, Galvan J, Myakov A, Lacy A, Lotan R, Richards-Kortum R (2002) Realistic three-dimensional epithelial tissue phantoms for biomedical optics. J Biomed Opt 7(1):148–156
39. Gossage KW, Smith CM, Kanter EM, Hariri LP, Stone AL, Rodriguez JJ (2006) Williams SK and Barton JK Texture analysis of speckle in optical coherence tomography images of tissue phantoms. Phys Med Biol 51:1563–1575
40. Vishwananth K, Pogue B, Mycek M (2002) Quantitative fluorescence lifetime spectroscopy in turbid media: comparison of theoretical, experimental and computational methods. Phys Med Biol 47:3387–3405
41. van Staveren HJ, Moes CJM, van Marle J (1991) Prahl SA and can Gemert MJC Light scattering in intralipid-10% in the wavelength range of 400-1100nm. Appl Opt 30(31):4507–4514
42. Luadi M, Colombo A, Farina B, Tomatis S, Marchesini R (2001) A phantom with tissue-like optical properties in the visible and near infrared for use on photomedicine. Las Sure Med 28:237–243
43. Germer C, Roggan A, Ritz JP, Isbert C, Albrecht D, Muller G, Buhr H (1998) Optical properties of native and coagulated human liver tissue and liver metastases in the near infrared range. Las Sure Med 23:194–203

44. Toricelli A, Pifferi A, Taroni P, Giambattistelli E, Cubeddu R (2001) In vivo optical characterization of human tissues from 610-1010nm by time-resolved reflectance spectroscopy. Phys Med Biol 46:2227–2237
45. Doornbos R, Lang R, Aalders M, Cross F, Sterenborg H (1999) The determination of in vivo human tissue optical properties and absolute chromophore concentrations using spatially resolved steady-state diffuse reflectance spectroscopy. Phys Med Biol 44:967–981
46. Welch AJ, Gardner C (2002) Optical and thermal response of tissue to laser radiation. Lasers Med Sci 27-45, edited by Waynant RW, CRC Press
47. Ishimaru A (1978) Wave propagation and scattering in random medium. Academic Press, New York
48. Hornung R, Pham TH, Keefe KA, Berns MW, Tadir Y, Tromberg BJ (1999) Quantitative near-infrared spectroscopy of cervical dysplasia in vivo. Human Reprod 14(11):2908–2916
49. Matsumura Y, Maeda H (1986) A new concept of macromolecular therapies in cancer chemotherapy: mechanism of tumor tropic accumulation of proteins and the anti-tumor agent SMANCS. Cancer Res 6:6387–6392
50. Maeda H, Wu J, Sawa T, Matsumura Y, Hori K (2000) Tumor vascular permeability and the EPR effect in macromolecular therapeutics: a review. J Contr Release 65:271–284
51. Maeda H (2001) The enhanced permeability and retention (EPR) affect in tumor vasculature: the key role of tumor-selective macromolecular drug targeting. Adv Enzym Regul 41:189–207
52. Maeda H, Fang J, Inutsuka T, Kitamoto Y (2003) Vascular permeability enhancement in solid tumor: various factors, mechanisms involved and its implications. Int Immunopharmacol 3: 319–328
53. Iyer A, Khaled G, Fang J, Maeda H (2006) Exploiting the enhanced permeability and retention effect for tumor targeting. Drug Discov Today 11:812–818